

pubs.acs.org/JPCA Article

Molecular Design of Heptazine-Based Photocatalysts: Effect of Substituents on Photocatalytic Efficiency and Photostability

Johannes Ehrmaier, Xiang Huang, Emily J. Rabe, Kathryn L. Corp, Cody W. Schlenker, Andrzej L. Sobolewski, and Wolfgang Domcke*



Cite This: J. Phys. Chem. A 2020, 124, 3698–3710



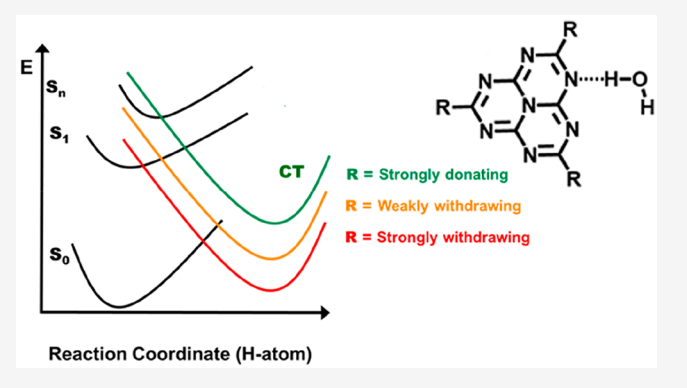
ACCESS

III Metrics & More

Article Recommendations

s Supporting Information

ABSTRACT: Recently, a derivative of the heptazine (tris-triazine) molecule, trianisole-heptazine (TAHz), was synthesized and was shown to catalyze the oxidation of water to hydroxyl radicals under 365 nm LED light in a homogeneous reaction (E. J. Rabe et al., J. Phys. Chem. Lett. 2018, 9, 6257–6261). The possibility of water photo-oxidation with a precisely defined molecular catalyst in neat solvents opens new perspectives for clarifying the fundamental reaction mechanisms involved in water oxidation photocatalysis. In the present work, the effects of chemical substituents on the three CH positions of Hz on the photocatalytic reactivity were explored with wave function-based *ab initio* electronic-structure calculations for hydrogen-bonded complexes of Hz and three selected Hz derivatives (TAHz, trichloro-Hz, and tricyano-Hz) with a water



molecule. While anisole is an electron-donating substituent, Cl is a weakly electron-withdrawing substituent and CN is a strongly electron-withdrawing substituent. It is shown that the barrier for the photoinduced abstraction of an H atom from the water molecule is raised (lowered) by electron-donating (electron-withdrawing) substituents. The highly mobile and reactive hydroxyl radicals generated by water oxidation can recombine with the reduced chromophore radicals to yield photohydrates. The effect of substituents on the thermodynamics of the photohydration reaction was computed. Among the four chromophores studied, TAHz stands out on account of the metastability of its photohydrate, which suggests self-healing of the photocatalyst after oxidation of TAHzH radicals by OH radicals. In addition, the effect of substituents on the H atom photodetachment reaction from the reduced chromophores, which closes the catalytic cycle, has been investigated. The energy of the repulsive $^2\pi\sigma^*$ state, which drives the photodetachment reaction is lowered (raised) by electron-donating (electron withdrawing) substituents. All four chromophores exhibit inverted S_1/T_1 gaps. This feature eliminates long-lived triplet states and thus avoids the activation of molecular oxygen to highly reactive singlet oxygen.

1. INTRODUCTION

The past ten years witnessed a remarkable surge of interest in polymeric carbon nitride materials as catalysts for the light-driven evolution of molecular hydrogen. $^{1-4}$ These carbon nitride materials, consisting of triazine (Tz) or heptazine (Hz) building blocks, 5 contain only earth-abundant elements, are easily prepared from simple precursors by high-temperature/high-pressure pyrolysis, and exhibit a surprisingly high degree of photostability. $^{1-3}$ The most commonly used material, generally referred to as melon or graphitic carbon nitride (g-C₃N₄), 5 consists of chains of Hz units that are connected by imide groups. The chemical composition and the molecular structure of the materials depend on the preparation conditions and therefore are not precisely defined, which is a disadvantage for the exploration of the fundamental reaction mechanisms.

The isolated Hz molecule was synthesized by Hosmane et al. in 1982 and its structure, proposed by Pauling and Surdivant in

1937, was confirmed by X-ray crystallography. Hz hydrolyzes rapidly in the presence of traces of water and light and therefore is not readily available. Recently, Schlenker and coworkers synthesized a Hz derivative, trianisole-heptazine (TAHz), which is chemically easier to handle than Hz (for reasons explained below) and investigated its spectroscopy and photoreactivity. TAHz in toluene was found to exhibit an exceptionally long lifetime of the S₁ state (287 ns) and a high fluorescence quantum yield (69%). TAHz suspensions in water, however, were found to exhibit a much shorter S₁ lifetime of 19 ns. Moreover, a short-lived (190 ps) transient

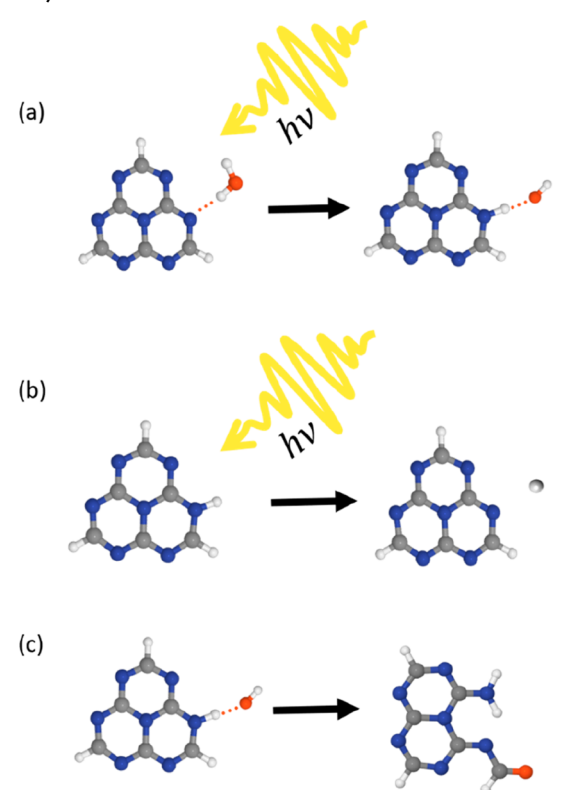
Received: January 17, 2020 Revised: March 15, 2020 Published: April 21, 2020





blue-shifted fluorescence violating Kasha's rule was detected for TAHz in water by global target analysis. The blue-shifted fluorescence was found to exhibit a kinetic isotope effect of 2.9 in D_2O vs H_2O , which is a clear indication that the excited state is quenched by PCET from water to the chromophore. The photoinduced oxidation of water molecules (see Scheme 1a) was confirmed by the detection of the photogenerated free

Scheme 1. (a) A Photon Triggers the H atom Transfer Reaction from Water to the Hz Chromophore, Forming the HzH···OH Radical Pair; (b) Photodetachment of the Excess Hydrogen Atom Occurs from the HzH Radical; (c) HzH and OH Radicals Recombine in a Dark Reaction To Form Photohydrates of Hz



OH radicals (using terephthalic acid as OH radical scavenger and fluorescence marker). These findings have two important implications. (i) A molecular chromophore in solution can oxidize water (that is, neither aggregation nor solid-state transport processes are *a priori* essential) and (ii) the TAHz chromophore indeed can oxidize water molecules with near-UV light, not just sacrificial electron donors with low oxidation potentials. The mechanistic details of the photochemical water oxidation reaction can thus be investigated for a precisely defined chromophore in neat solvents, which opens exciting perspectives for comprehensive and precise joint experimental/ theoretical studies of the reaction mechanisms.

In recent work, the wide range of oxidation potentials for para-substituted phenol derivatives (R-PhOH, R = H, Cl, Br, CN, CH₃, OCH₃) and the solubility of TAHz in toluene were exploited to systematically investigate the dependence of the hydrogen-bonding association constant and the excited-state PCET reaction rate on the oxidation potential of the electron donor. ¹⁰ Electron-donating substituents, such as CH₃ (Me) or OCH₃ (MeO), lower the oxidation potential of the electron donor, while electron-withdrawing substituents, such as Cl, Br,

or CN, increase the oxidation potential of the electron donor. The rate constant for excited-state PCET from phenol to TAHz was found to increase by a factor of about 10 from the most electron-withdrawing substituent to the most electron-donating substituent on phenol. The measured PCET time constant was found to scale approximately linearly with the *ab initio* computed PCET barrier on the S₁ PE surface of the TAHz···R—PhOH complexes. These combined experimental and computational findings provide convincing evidence that the excited-state quenching in TAHz···R—PhOH complexes occurs by excited-state PCET. Remarkably, a completely barrierless PCET reaction is theoretically predicted for the phenol derivative with the lowest oxidation potential (MeO—PhOH) and is confirmed by the experimental data. ¹⁰

In the present work, we address with ab initio computational studies the complementary possibility of chemical substitution, namely, the role of substituents on the three CH positions of the Hz chromophore for the excited-state PCET reactivity in complexes with water molecules. In the order of increasing complexity, the selected chromophores are Hz, trichloroheptazine (cyanuric chloride, TClHz), tricyano-heptazine (TCNHz), and TAHz. While anisole is an electron-donating substituent, Cl and CN are moderately and strongly electronwithdrawing substituents, respectively. It is expected that TAHz exhibits a lower reduction potential than Hz, whereas TClHz and in particular TCNHz should exhibit increased reduction potentials. We emphasize that we are concerned here with substitutions on the carbon atoms of Hz itself. These substituted Hz compounds should not be confused with substituted melem (triamino-heptazine) compounds, such as cyanamides of Hz, which were discussed in the literature. 11-Since the strongly electron-donating amino groups of melem cause a substantial (about 1.0 eV) blue shift of locally excited (LE) and charge-transfer (CT) states, 14 melem and its derivatives are less attractive chromophores for solar water oxidation than Hz and its derivatives.

The focus of the present investigation is on the vertical excitation energies of LE and CT excited states and on the topography of the electronic PE surfaces involved in the PCET reaction in hydrogen-bonded complexes of these chromophores with a single water molecule. Admittedly, complexes of a chromophore with a single water molecule are minimalistic models for the investigation of the aqueous photochemistry of these chromophores. In previous ab initio computational studies, excited-state PE surfaces and the associated nonadiabatic excited-state dynamics were explored for complexes of the pyridine molecule with up to five water molecules. 15,16 Alternatively, the photodynamics of a Hz molecule in a liquidwater environment, modeled by 120 water molecules with periodic boundary conditions, was studied with density functional theory (DFT) and time-dependent density functional theory (TDDFT).¹⁷ These studies showed that the most essential aspects of the excited-state PE surfaces for PCET are well represented by complexes of the chromophore with a single water molecule. For the simulation of the photoinduced nonadiabatic reaction dynamics, however, it is necessary to include at least a handful of water molecules to allow for efficient dissipation of the excess energy of the PCET reaction. 16,18

2. COMPUTATIONAL METHODS

The geometries of the Hz···H₂O, TClHz···H₂O, TCNHz··· H₂O, and TAHz···H₂O complexes were determined by

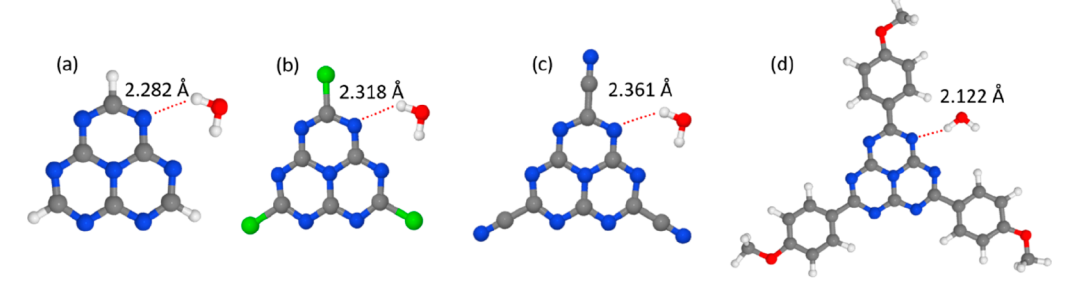


Figure 1. Equilibrium geometries of Hz and three Hz derivatives with a hydrogen-bonded water molecule: (a) Hz···H₂O, (b) TClHz···H₂O, (c) TCNHz···H₂O, and (d) TAHz···H₂O. The length of the hydrogen bond is specified.

minimizing the energy of the electronic ground state with second-order Møller-Plesset perturbation theory (MP2). The equilibrium geometries of the Hz···H₂O, TClHz···H₂O, and TCNHz···H₂O complexes were optimized without symmetry constraint and were found to exhibit C_s symmetry. For the TAHz-H₂O complex, C_s symmetry was enforced for technical reasons (to speed up convergence of the geometry optimization). Vertical electronic excitation energies were evaluated at the ground-state equilibrium geometries with the second-order algebraic-diagrammatic-construction scheme (ADC(2)),²⁰ which is a computationally efficient singlereference propagator method. The ADC(2) method provides a balanced description of the energies of LE states of the chromophore and of water-to-chromophore CT states, which is essential for a reliable characterization of the PE surfaces of PCET reactions.

PCET reactions involve the breaking and making of chemical bonds. Multiconfigurational multireference methods would be ideal for the computation of PE surfaces of photochemically reactive systems, but for systems of the size considered here such methods are not feasible for geometry optimizations of excited electronic states. Instead, one has to make intelligent use of computationally efficient singlereference methods. The reference state in the present calculations is the closed-shell state, which is the electronic ground state in the vicinity of the equilibrium geometry of the chromophore—water complex. The lowest ${}^{1}\pi\pi^{*}$ excited state in the Franck-Condon region and the lowest biradical state in the product region are both open-shell states and their orbitals and configurations change smoothly along the reaction coordinate. The one-dimensional and two-dimensional relaxed scans were computed with the closed-shell reference state. Excitation energies become negative in certain regions of nuclear coordinate space. C_s symmetry is very helpful for these calculations, since it excludes perturbations arising from interactions between $\pi\pi^*$ (A' symmetry) and $n\pi^*$ (A" symmetry) states. When the energy gap between the openshell ground state and closed-shell excited state gets very large (such as for TCNHz-H₂O at large OH distances), it can happen that the Hartree-Fock calculation for the high-energy closed-shell reference fails to converge. However, this case is exceptional and in general the Hartree-Fock calculations converge smoothly when carefully chosen initial guesses are used by propagating the electronic-structure calculation in sufficiently small steps along the reaction coordinate(s).

The accuracy of the MP2 and ADC(2) methods for PE surfaces of PCET reactions was evaluated in previous studies in comparison with multiconfiguration multireference methods (CASSCF/CASPT2) for pyridine– H_2O and triazine– H_2O

complexes. The MP2 and ADC(2) methods were found to be reliable tools for the description of photoinduced H atom transfer reactions from water molecules to N-heterocyclic chromophores.^{21–23}

One-dimensional relaxed PE profiles were computed along the H atom transfer reaction coordinate. The OH bond length of the water molecule involved in hydrogen bonding with the chromophore was kept fixed, while all other nuclear degrees of freedom of the complex were optimized in order to minimize either the ground-state energy (ground-state reaction path) or the energy of the lowest excited singlet state (excited-state reaction path). The second OH bond length of the water molecule was also kept fixed during the geometry optimization of the S_1 state to avoid unwanted side reactions. For all excited-state geometry optimizations, C_s symmetry was imposed. The energies of the other electronic states were calculated as single-point energies at the optimized geometries.

Two-dimensional relaxed PE surfaces were computed by fixing the OH bond length of the water molecule and the distance of the oxygen atom of water from the accepting nitrogen atom of the chromophore, while all other nuclear degrees of freedom of the complex (except the second OH-distance of the water molecule), were relaxed in order to minimize the energy of the lowest excited singlet state with C_s symmetry constraint.

Equilibrium geometries of the S_1 state of the complexes were obtained by geometry optimization with C_s symmetry constraint. The location of the saddle point of the excited-state PCET reaction was estimated by inspection of the two-dimensional relaxed PE surfaces. With this geometry as an initial guess, the saddle point geometry has been fully optimized and the Hessian was computed. It was verified that the Hessian exhibits a single imaginary frequency and that the corresponding eigenvector represents an H atom transfer reaction.

For the exploration of the ground-state and excited-state PE surfaces of the reduced chromophore radicals (HzH, TClHzH, TCNHzH, TAHzH), the unrestricted versions of the MP2 method and the ADC(2) method,²⁴ respectively, were employed. The energy profiles of the ground state and of the lowest excited states were computed as rigid scans along the NH stretching coordinate.

Dunning's correlation-consistent double- ξ basis set (cc-pVDZ)²⁵ was employed for the chromophore–water complexes. For the reduced chromophore radicals, the augmented double- ξ basis set (aug-cc-pVDZ) was used. The calculations were performed with the TURBOMOLE program package²⁶ using the resolution-of-the-identity approximation.²⁷

3. RESULTS

3.1. Equilibrium Structures and Vertical Excitation **Energies.** The equilibrium geometries of the Hz···H₂O, TClHz···H2O, TCNHz···H2O, and TAHz···H2O complexes are shown in Figure 1. The chromophore-water hydrogenbond lengths are specified in the figure. Alternative equilibrium structures with the molecular plane of the water molecule oriented perpendicular to the molecular plane of the chromophore exist but were not considered in the present work. These structures are essentially isoenergetic with the structures with in-plane oriented water molecules. From TAHz···H₂O via Hz···H₂O to TCNHz···H₂O, a systematic and substantial increase of the hydrogen-bond length between the chromophore and the water molecule is observed, from 2.122 to 2.361 Å. The higher the electron-donating character of the substituent on the Hz core, the higher is the electronic density on the peripheral nitrogen atoms. An increased electronic density on the N atoms gives rise to a stronger hydrogen bond with the water molecule.

The vertical excitation energies of the lowest seven LE singlet electronic states as well as the vertical excitation energy of the lowest water-to-chromophore CT state are listed in Table 1. The corresponding oscillator strengths are displayed

Table 1. Vertical Excitation Energies (in eV) of the Lowest Seven LE Singlet Excited States and the CT State of Hydrogen-Bonded Complexes of Hz and Three Hz Derivatives with a Water Molecule, Calculated with the ADC(2) Method^a

$Hz\cdots H_2O$	$TClHz\cdots H_2O$	$TCNHz\cdots H_2O$	$TAHz \cdots H_2O$
S ₁ (ππ*) 2.59 (0.0000)	$S_1(\pi\pi^*)$ 2.79 (0.0001)	$S_1(\pi\pi^*)$ 2.33 (0.0001)	$S_1(\pi\pi^*)$ 2.65 (0.0013)
S ₂ (nπ*) 3.77 (0.0000)	S ₂ (nπ*) 3.91 (0.0000)	S ₂ (nπ*) 3.43 (0.0000)	$S_2(\pi\pi^*)$ 3.50 (1.0829)
S ₃ (nπ*) 3.85 (0.0000)	S ₃ (nπ*) 3.99 (0.0000)	S ₃ (nπ*) 3.51 (0.0000)	$S_3(\pi\pi^*)$ 3.59 (1.2080)
S ₄ (nπ*) 3.91 (0.0000)	S ₄ (nπ*) 4.03 (0.0000)	S ₄ (nπ*) 3.55 (0.0000)	S ₄ (nπ*) 3.71 (0.0000)
$S_5(\pi\pi^*)$ 4.43 (0.2578)	$S_5(\pi\pi^*)$ 4.48 (0.3250)	S ₅ (CT) 4.13 (0.0001)	S ₅ (nπ*) 3.79 (0.0000)
$S_6(\pi\pi^*)$ 4.43 (0.2832)	$S_6(\pi\pi^*)$ 4.48 (0.2964)	S ₆ (ππ*) 4.16 (0.3111)	S ₆ (nπ*) 3.89 (0.0000)
S ₇ (nπ*) 4.89 (0.0022)	S ₇ (nπ*) 4.92 (0.0023)	$S_7(\pi\pi^*)$ 4.17 (0.2865)	$S_7(\pi\pi^*)$ 3.96 (0.0264)
S ₁₃ (CT) 5.40 (0.0019)	S ₈ (CT) 4.96 (0.0024)	S ₈ (nπ*) 4.66 (0.0009)	S _n (CT) 6.15 (0.0369)

^aOscillator strengths are given in parentheses. Ground-state equilibrium geometries were determined with the MP2 method.

in parentheses. In the $Hz\cdots H_2O$ and $TClHz\cdots H_2O$ complexes, the low-lying $S_1(\pi\pi^*)$ state is followed by three essentially dark $^1n\pi^*$ states and a nearly degenerate pair ($^1E'$ symmetry for isolated Hz) of strongly dipole-allowed $^1\pi\pi^*$ states. S_7 is a weakly allowed $^1\pi\pi^*$ state. In the $TAHz\cdots H_2O$ complex, the energy of the bright $^1\pi\pi^*$ pair is significantly red-shifted, which is the consequence of the excitonic interaction between the bright $^1\pi\pi^*$ state of the Hz core and the $^1\pi\pi^*$ states of the anisole substituents. The CT state, however, is strongly blue-shifted to 6.15 eV in TAHz, which reflects the electron-donating character of anisole. In the $TCNHz\cdots H_2O$ complex, the bright $^1\pi\pi^*$ pair is only weakly red-shifted, while the energy of the CT state is strongly down-shifted to 4.13 eV. The strong variation of the energy of the CT state among the four systems

(between 4.13 and 6.15 eV) is remarkable and will be discussed in more detail below.

The low-lying dark $S_1(\pi\pi^*)$ state is a specific feature of the Hz chromophore. 28 The S₁ state corresponds to a nearly pure HOMO-to-LUMO excitation of the Hz core. The HOMO and the LUMO of the four complexes are depicted in Figure 2. The HOMO is located on the peripheral nitrogen atoms, while the LUMO is located on the carbon atoms and on the central nitrogen atom. HOMO and LUMO have almost no spatial overlap, which leads to an unusually small exchange integral (0.125 eV for isolated Hz). It has recently been shown that the small exchange integral combined with substantial spin polarization²⁹ leads to an inversion of the energies of the S₁ and T₁ states, the T₁ state being located about 0.25 eV above the S₁ state.³⁰ The relevance of this unique feature of Hz and Hz derivatives for water-oxidation photocatalysis will be discussed below. The vertical excitation energies of the S₁ state of the complexes of Hz, TClHz, TCNHz, and TAHz with a water molecule differ by about 0.5 eV, with TCNHz···H₂O (2.33 eV) at the lower end and TClHz···H₂O (2.79 eV) at the upper end.

3.2. Energy Profiles of the Minimum-Energy Reaction Path for PCET. PE profiles (relaxed scans) for the excitedstate H atom transfer reaction from the water molecule to the chromophore are displayed in Figure 3a-d. The reaction coordinate R_{OH} is the OH bond length of the hydrogenbonded water molecule. Each figure consists of two parts. For small OH bond lengths ($R_{\rm OH}$ < 1.2 Å, left part), the energy of the ground state was minimized for fixed R_{OH} (black dots). The energies of the excited electronic states were obtained by single-point calculations at the S₀-optimized geometries (circles). States of $\pi\pi^*$ character are depicted in green; states of $n\pi^*$ character are depicted in red. For large OH distances ($R_{\rm OH}$ > 1.2 Å, right part), the energy of the lowest excited state of A' symmetry was optimized for fixed R_{OH} (blue dots). The energy of the closed-shell electronic ground state has been calculated at the excited-state optimized geometries (black circles). In most of this region, the lowest state of A' symmetry is the water-to-chromophore CT state. In the CT state, an electron is transferred from the p, orbital of water to the chromophore (filling the hole in the HOMO of the chromophore). The transfer of the electron (leading to a negatively charged chromophore and a positively charged water molecule) provides the driving force for the transfer of the proton from the water molecule to the chromophore. The result is a neutral biradical system, consisting of the reduced (hydrogenated) chromophore radical and the OH radical (see Scheme 1a). The biradical is the lowest electronic state for R_{OH} > 1.4 Å and represents, at its equilibrium geometry, a chemically stable species. It should be noted that the PE profile of the biradical is repulsive with respect to the backtransfer of electron and proton, which prevents back-transfer, provided the excess energy of the electron/proton transfer reaction can efficiently be dissipated to an environment. In the complexes of Hz, TClHz, and TAHz with H2O, about 2.0 eV (46 kcal/mol) are stored as chemical energy in the biradical. In TCNHz···H₂O, the energy of the biradical is particularly low and only about 1.0 eV (23 kcal/mol) of chemical energy are stored in the biradical.

In the left region ($R_{\rm OH}$ < 1.2 Å), the PE profiles of the lowest seven excited states, which are LE states of the chromophore, are essentially parallel to the ground-state energy profile. In other words, the shifts of the equilibrium geometries of the LE

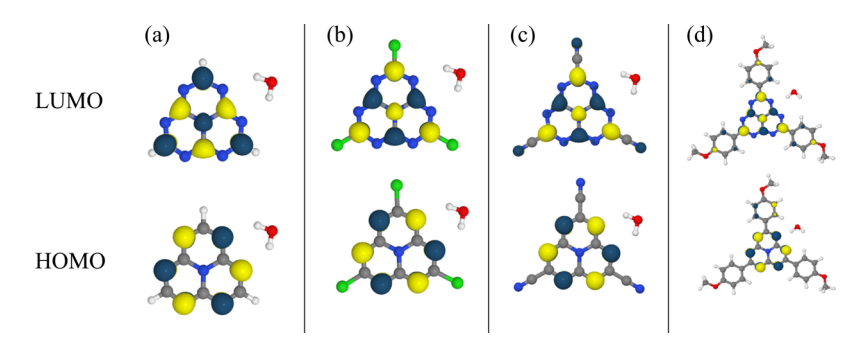


Figure 2. Lowest unoccupied Hartree–Fock molecular orbital (LUMO) and highest occupied molecular orbital (HOMO) for (a) $Hz\cdots H_2O$, (b) $TClHz\cdots H_2O$, (c) $TCNHz\cdots H_2O$, and (d) $TAHz\cdots H_2O$. The S_1 states of $Hz\cdots H_2O$, $TClHz\cdots H_2O$, and $TCNHz\cdots H_2O$ are nearly pure HOMO–LUMO excitations. In TAHz, the S_1 state corresponds to the excitation from HOMO–4 to the LUMO. The orbital shown in the lower frame of (d) is the HOMO–4.

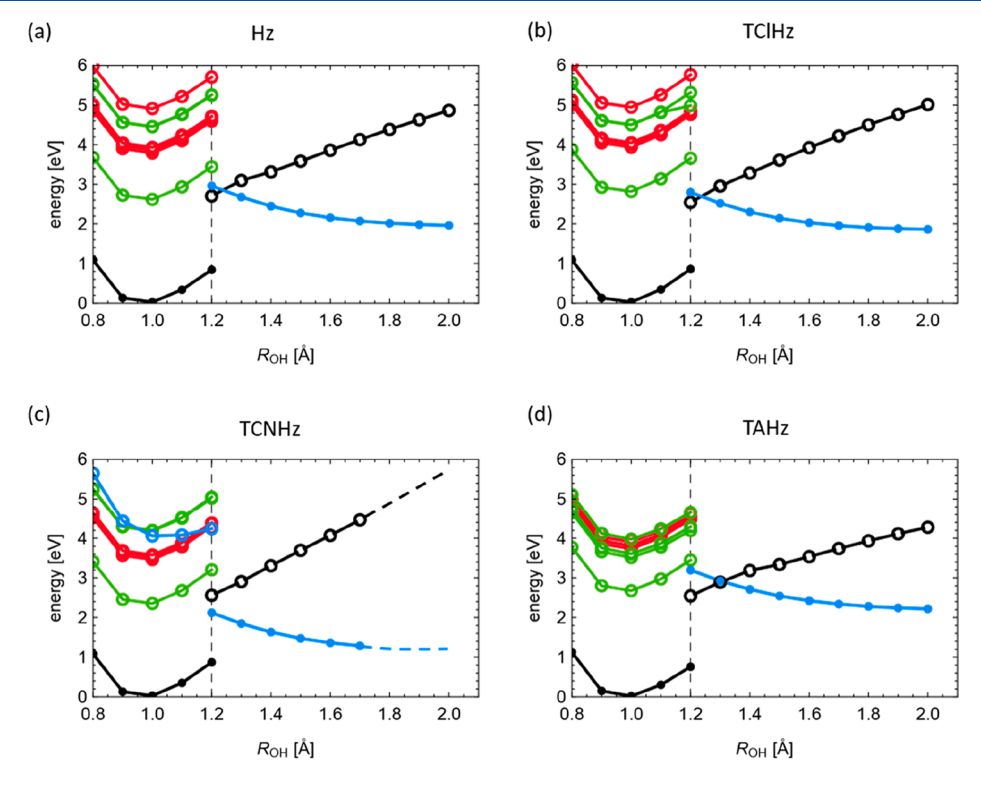


Figure 3. Energy profiles of relaxed scans for the H atom transfer reaction from water to (a) Hz, (b) TClHz, (c) TCNHz, and (d) TAHz. For R_{OH} < 1.2 Å the energy of the electronic ground state (black) was optimized, while for R_{OH} > 1.2 Å the energy of the CT state (blue) was optimized. LE $\pi\pi^*$ states are shown in green; LE $n\pi^*$ states, in red.

states are essentially zero (Figure 3a,b,d). The TCNHz···H₂O complex (Figure 3c) represents an exception. Here the CT state (blue) is embedded in the manifold of LE states and its energy is sensitive to the location of the proton. For the TAHz···H₂O complex (Figure 3d), the bright $\pi\pi^*$ states are red-shifted relative to the Hz···H₂O complex (Figure 3a) and ADC(2) predicts them to be located slightly below the $n\pi^*$ states. The experimental absorption spectrum of TAHz in aqueous solution, however, reveals the lowest $n\pi^*$ states slightly below the lowest bright $n\pi^*$ state. The error of about 0.2 eV in the relative energies of LE $n\pi^*$ and $n\pi^*$ states is within the expected error margin of the ADC(2) method.

The crossing of the energy of the CT state (blue) with the energy of the S_0 state (black) in Figure 3a–c represents a conical intersection³¹ of two singlet states of the same symmetry. The point of intersection shifts toward smaller $R_{\rm OH}$ and to lower energies for electron-withdrawing sub-

stituents. For TAHz··· H_2O , the energy crossing occurs at R_{OH} = 1.30 Å and an energy of 2.92 eV, for Hz···H₂O and TClHz··· H_2O , it is located at $R_{OH} = 1.24$ Å and 2.70–2.80 eV, and for TCNHz···H₂O, it is at R_{OH} < 1.2 Å. Electron-withdrawing groups induce a red shift of the CT state that leads to crossings with the S₀ energy at smaller OH bond lengths and lower energies. In the TCNHz···H₂O complex, the ground-state energy is particularly strongly destabilized by the H atom transfer reaction. As a consequence, the restricted Hartree-Fock and MP2 calculations did not converge for $R_{\rm OH} > 1.7~{\rm \AA}$ and the PE profiles had to be extrapolated (dashed blue and black lines in Figure 3c). Altogether, for all four systems, the existence of a chemically stable biradical species has been established. Electron-donating substituents on Hz increase the energy of the biradical, while electron-withdrawing substituents on Hz lower the energy of the biradical and shift the conical intersection with the S_0 state toward smaller OH bond lengths.

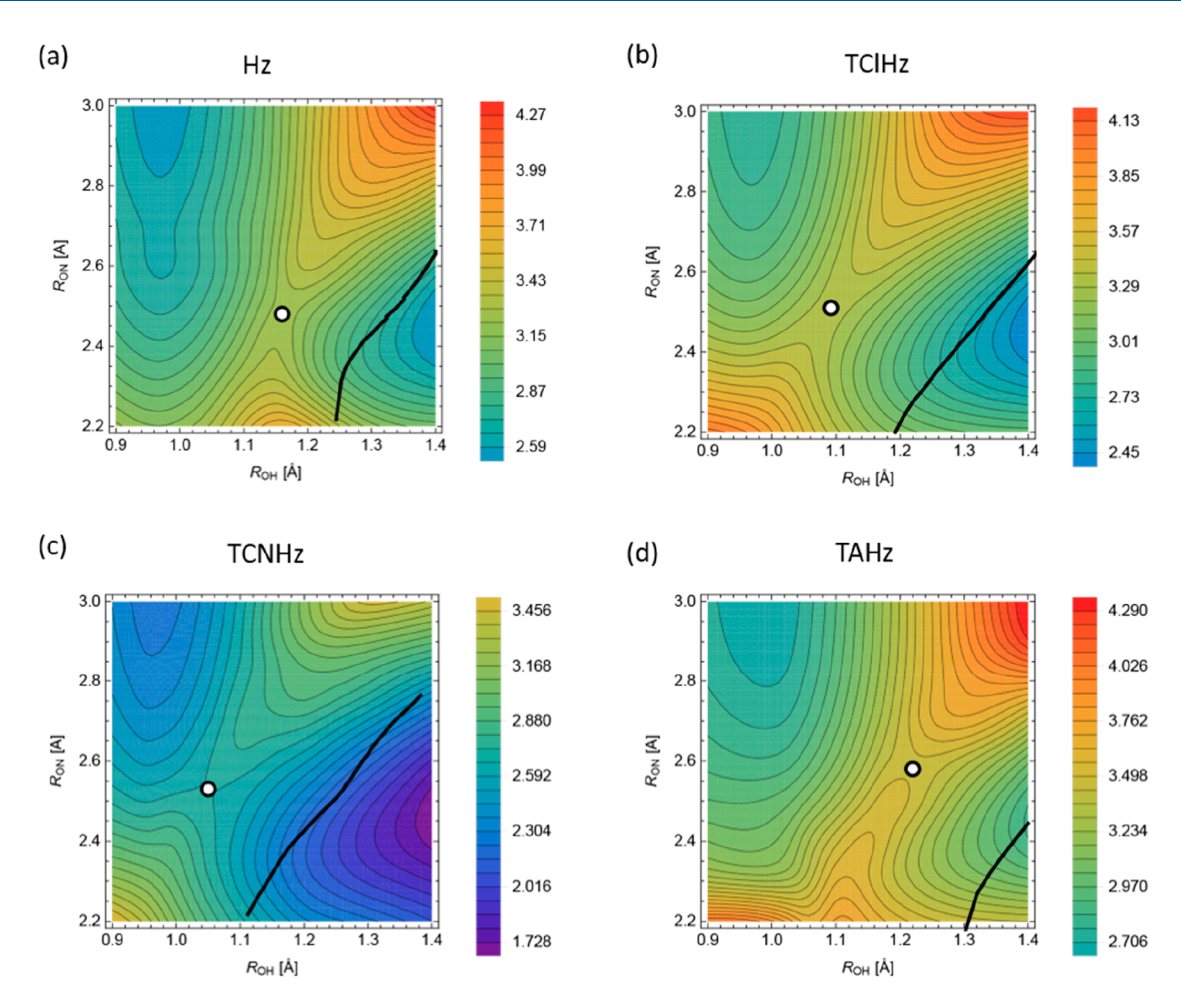


Figure 4. Two-dimensional relaxed PE surfaces of the S_1 state of the (a) $Hz\cdots H_2O$, (b) $TCHz\cdots H_2O$, (c) $TCNHz\cdots H_2O$, and (d) $TAHz\cdots H_2O$ complexes. The saddle point is marked by the circle. The black line represents the crossing seam of the PE surface of the open-shell S_1 state with the PE surface of the closed-shell S_0 state. Energies are given in electronvolts relative to the energy minimum of the S_0 state.

3.3. Two-Dimensional PE Surfaces and PCET Barrier.

Two-dimensional relaxed PE surfaces relevant for the PCET reaction in the adiabatic S₁ state of the chromophore-water complexes were computed as described in section 2. The relaxed two-dimensional PE surfaces of the four complexes are displayed in Figure 4a-d. The reaction coordinates are R_{OH} , as in the one-dimensional relaxed scans of Figure 3, and the distance R_{ON} of the O atom of water from the accepting N atom of the chromophore (see Scheme 1a). For all systems, the adiabatic PE surface of the S₁ state exhibits two minima. The minimum for small $R_{\rm OH}$ and large $R_{\rm ON}$ is located in the Franck-Condon region of the chromophore and corresponds to the energy minimum of the LE $S_1(\pi\pi^*)$ state. It is only minimally shifted with respect to the ground-state equilibrium geometry. The second minimum is located at large $R_{\rm OH}$ and small R_{ON} and corresponds to the equilibrium geometry of the biradical. The two minima are separated by a saddle point that is indicated by the circle in Figure 4a-d. The Cartesian coordinates of these saddle points are reported in the Supporting Information. At this saddle point, the adiabatic S₁ electronic wave function changes character from LE($\pi\pi^*$) to water-to-chromophore $CT(\pi\pi^*)$. The OH bond length of the saddle point decreases systematically with increasing electronwithdrawing character of the substituent from $R_{OH} = 1.22 \text{ Å for}$ TAHz to $R_{OH} = 1.05$ Å for TCNHz. The latter value

corresponds to a stretching of the OH bond length from the ground-state equilibrium geometry by merely 0.05 Å.

The energy difference between the energy minimum of the LE S_1 state and the saddle point defines the height of the barrier for the PCET reaction. The energies of the LE S_1 minimum, the energy of the saddle point, and the barrier height are listed in Table 2. The energies of the S_1 minima are

Table 2. Minimum-to-Minimum Excitation Energy of the LE S₁ State, Energy of the Saddle Point, and Corresponding Barrier Height of the PCET Reaction for the Hz···H₂O, TClHz···H₂O, TCNHz···H₂O, and TAHz····H₂O Complexes (All Energies in Electronvolts)

	Hz	TClHz	TCNHz	TAHz
S_1 minimum	2.51	2.71	2.23	2.58
saddle point	3.49	3.51	2.82	3.66
barrier height	0.98	0.80	0.59	1.08

stabilized by less than 0.1 eV compared to the vertical excitation energies (cf. Table 1), revealing weak electron-vibrational coupling in the LE $\pi\pi^*$ state. The PCET reaction barrier of the reference complex Hz···H₂O is 0.98 eV. The electron-donating substituent anisole increases the barrier to 1.08 eV. The strongly electron-withdrawing substituent CN, however, lowers the barrier to 0.59 eV. The barrier height can

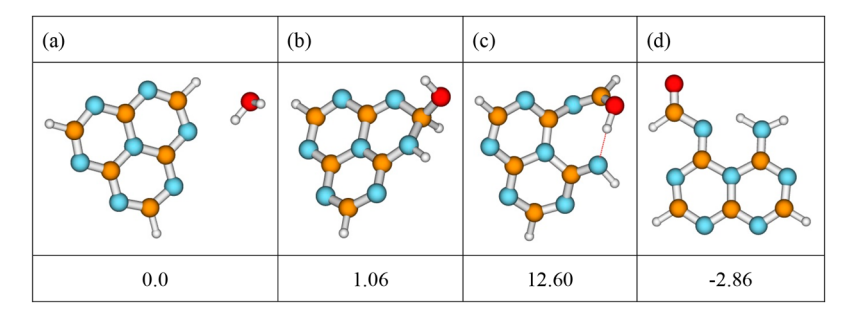


Figure 5. Structures of and relative energies (in kcal/mol) of photohydrates of Hz, computed at the MP2/cc-pVDZ level.

Table 3. Energies of the Intermediate Photohydrate (Middle Column) and the Thermodynamically Most Stable Photohydrate (Right Column) Relative to the Energy of the Chromophore–Water Complex (Left Column) for Hz···H₂O, TClHz···H₂O, TCNHz···H₂O, and TAHz···H₂O, Calculated at the MP2/cc-pVDZ Level

X N N OH ₂	X OH NH NH N X	O NH ₂ N N N N N N N N N N N N N N N N N N N
Х	ΔE (kcal/mol)	Δ E(kcal/mol)
· · · · · · · · · · · · · · · · · · ·		
Н	1.06	-2.86
H Cl	1.06 -5.98	-2.86 -5.32

thus be tuned by nearly 0.5 eV by varying the substituent on the Hz chromophore. Since the tunneling rate through the barrier depends exponentially on the barrier height, this implies a very significant dependence of the PCET reaction rate on the substituent. The zero-point energy of the OH vibration can be estimated as 0.20 eV. In the TCNHz···H₂O complex, the PCET barrier is therefore about 0.39 eV higher than the zero-point energy, which suggests a tunneling rate in the picosecond regime.

The black line in Figure 4a-d represents the crossing seam of the S_1 and S_0 PE surfaces, that is, the line of S_1-S_0 conical intersection. This crossing seam is the one-dimensional extension of the zero-dimensional point of intersection of the blue and black PE profiles in Figure 3a-d. The location of the seam of the S_1-S_0 intersection is displaced to larger R_{OH} and to higher energies by the electron-donating substituent anisole (Figure 4d). However, the seam is shifted to smaller R_{OH} and lower energies by the electron-withdrawing substituent CN (Figure 4c). The location of the conical seam in nuclear coordinate space and in energy is relevant for the branching ratio of the PCET reaction (successful vs aborted H atom transfer), although the effects of the location and of properties (e.g., g, h vectors) of the seam are less obvious than in the case of the PCET barrier. To explore the effect of substituents on the branching ratio of the PCET reaction, nonadiabatic dynamics simulations have to be performed for chromophores in water clusters or in aqueous solution.

3.4. Thermochemistry and Spectroscopy of Photohydrates. The PCET reaction in the $Hz\cdots H_2O$ complex, if not aborted at the S_1-S_0 conical intersection seam, generates the $HzH\cdots OH$ biradical (see Scheme 1a). Since the excess energy of the PCET reaction (about 2.0 eV, i.e., 46.1 kcal/mol) is significantly larger than the binding energy of the $HzH\cdots OH$ hydrogen bond, the PCET reaction will yield free

HzH and OH radicals. If the reaction occurs in a large water cluster or in liquid aqueous solution, the two radicals may separate by diffusion. However, the OH radical is highly mobile and reactive and may also attach to one of the CH groups of Hz, forming a covalent bond, which corresponds to a nonadiabatic transition from the biradicalic electronic configuration to a closed-shell electronic configuration (see Scheme 1c).32 The molecular structure of the HzH-OH covalent adduct, optimized at the MP2 level, is shown in Figure 5b. This adduct is a so-called photohydrate³³ of Hz and its energy is only slightly higher (1.06 kcal/mol) than the energy of the Hz···H₂O complex. The attachment of the OH group to the carbon atom weakens the covalent bond with the neighboring nitrogen atom and a structure with broken C-N bond can be optimized at the MP2 level (Figure 5c). This photohydrate is about 12.60 kcal/mol higher in energy than the Hz···H₂O complex. Finally, an open amino-aldehyde photohydrate can be formed by the transfer of the hydrogen atom of the hydroxyl group to the imino group (Figure 5d). This H atom transfer reaction is exothermic and the amino-aldehyde photohydrate is found to be 2.86 kcal/mol more stable than the Hz···H₂O complex. Since this photohydrate is thermochemically stable, the photoinduced conversion of the Hz···H₂O complex to the photohydrate is an irreversible process. These results explain the well-known chemical instability of Hz in the presence of traces of water and light.8

We determined the structures of the photohydrates of TClHz, TCNHz, and TAHz and computed their relative energies; see Table 3. The energies of the amino—aldehyde forms of TClHz, TCNHz, and TAHz relative to the corresponding chromophore—water complexes are -5.32, -5.88, and +5.85 kcal/mol, respectively. The electron-withdrawing substituents Cl and CN stabilize the photohydrate, while the electron-donating anisole substituent

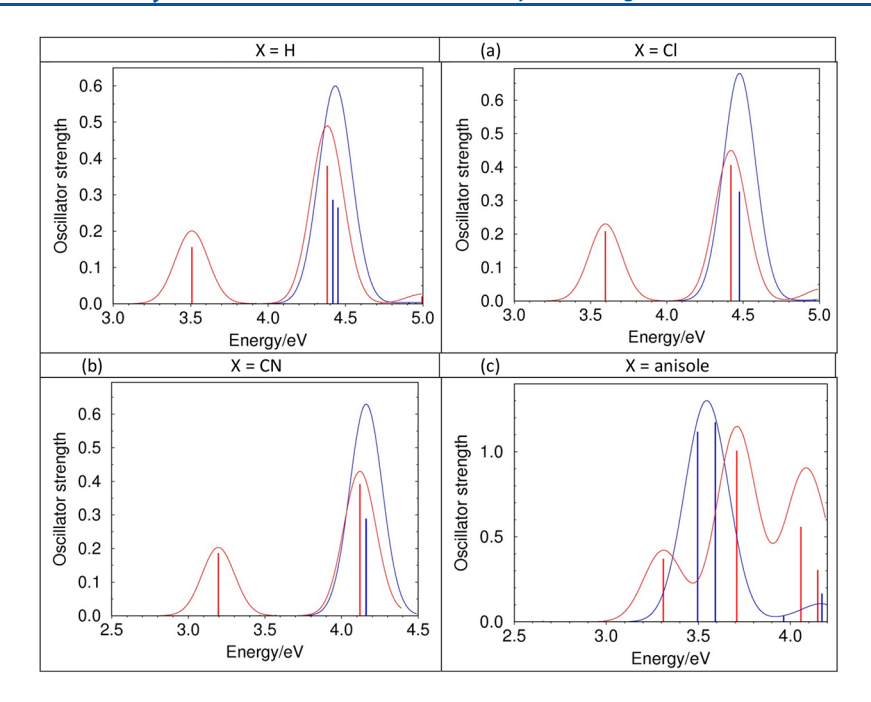


Figure 6. Simulated absorption spectra of the chromophore—water complex (blue sticks and envelopes) and the most stable photohydrate (red sticks and envelopes) for the (a) $Hz\cdots H_2O$, (b) $TCIHz\cdots H_2O$, (c) $TCNHz\cdots H_2O$, and (d) $TAHz\cdots H_2O$ complexes. The stick spectra were convoluted with a Gaussian of 0.5 eV fwhm.

destabilizes the photohydrate. Remarkably, the photohydrate of TAHz is higher in energy than the TAHz···H2O complex and therefore is metastable. The photohydrate will convert back to the TAHz···H₂O complex on a time scale determined by temperature and the lowest barrier separating the two ground-state structures. While further computational and experimental studies are necessary, the present results strongly suggest that TAHz may be a self-healing photocatalyst for water oxidation. Although the TAHz chromophore may be vulnerable to attack by photogenerated OH radicals, leading to the formation of photohydrates, the chromophore is spontaneously regenerated by a thermal reaction in the dark. It should be mentioned that TCNHz can alternatively react with water by the hydrolysis of the cyano groups. This reaction also is exothermic and presumably can occur even as a thermal ground-state reaction.

As is well-known for pyridine in aqueous solution, the formation and the decay of the photohydrate can be monitored by the measurement of the absorption spectra of pyridine and of the photohydrate.^{34,35} While pyridine absorbs in the far UV (255 nm), the open photohydrate of pyridine exhibits a strong absorption band in the near UV (\approx 360 nm). We simulated the absorption spectra of complexes of Hz, TClHz, TCNHz, and TAHz with a water molecule and the absorption spectra of the corresponding photohydrates by computing the vertical excitation energies and oscillator strengths with the ADC(2) method. The lines were convoluted with a Gaussian of 0.5 eV fwhm to simulate typical room-temperature solution spectra. These simulated spectra are displayed in Figure 6a-d. The absorption spectra of the chromophore-water complexes are shown by the blue sticks and the blue envelopes, while the spectra of the corresponding photohydrates are shown by the red sticks and the red envelopes.

It is seen that the complexes of Hz and TClHz with a water molecule absorb strongly near 4.4 eV (282 nm) (these numbers are approximate due to a systematic overestimation of

excitation energies by ADC(2) and the neglect of solvation effects). The TCNHz···H₂O complex absorbs near 4.2 eV (295 nm), while the absorption band of the TAHz···H₂O complex is red-shifted to about 3.5 eV (355 nm). For the complexes of Hz, TClHz, and TCNHz with a water molecule, the photohydrate absorbs at approximately the same wavelength as the chromophore. Other than in the pyridine—water system, the conversion of the Hz, TClHz, and TCNHz chromophores to the corresponding photohydrate is therefore not manifested by a bleaching of the characteristic absorption band of the chromophore. However, the photohydrates of Hz, TClHz, and TCNHz exhibit a new strong absorption band near 3.5 eV (355 nm), in a range where the chromophore-water complexes are transparent. By the measurement of the absorption of this band, the formation and decay of the photohydrate can be monitored. For the TAHz···H2O complex, however, the broad absorption of the photohydrate overlaps with the absorption band of the complex (see Figure 6d), which may prevent the spectroscopic detection of the photohydrate. It should also be mentioned that the photohydrates do not absorb at wavelengths longer than 400 nm and therefore are colorless. This excludes their back-conversion to the original chromophores by the absorption of visible light.

When TAHz suspensions in water were illuminated with a 365 nm laser at 2.7×10^{23} photons cm⁻² over 65 min, no significant loss of intensity of photoluminescence could be detected, suggesting that TAHz is not significantly degraded over the course of an hour. Moreover, when TAHz was employed for photodriven hydrogen evolution in aqueous suspension with 2 wt % platinum loading and TEOA as sacrificial electron donor,⁹ it was observed that the activity does not decrease over the course of 25 days of illumination. In fact, the hydrogen evolution rate increased over this period of time. This can presumably be attributed to the exfoliation of TAHz aggregates by illumination in aqueous solution, which results in greater effective chromophore concentration in

solution and/or larger aggregate surface area. TAHz therefore seems to exhibit excellent long-term stability under irradiation, similar as polymeric Hz-based materials, which is one of the reasons for the vast interest in these materials. Since Hz as well as TClHz (cyanuric chloride) hydrolyze rapidly in the presence of visible light, it is not trivial that molecular TAHz exhibits this high amount of long-term photostability. While it seems likely that the self-healing capacity of TAHz discussed above may contribute to its exceptional photostability, further investigations are necessary to unambiguously reveal the processes occurring under long-term irradiation of TAHz in the presence of water.

3.5. Recovery of the Chromophore by H atom Photodetachment. It has previously been shown that the pyridinyl (PyH), triazinyl (TzH), and heptazinyl (HzH) radicals possess low-lying $^2\pi\sigma^*$ excited states that play an important role in the photochemistry of these radicals. 21,22,28 The PE profiles of these $^2\pi\sigma^*$ excited states are, apart from a low barrier, repulsive along the N-H stretching coordinate. While the binding energy of the NH bond is of the order of 5.0 eV in the diabatic ground state of these radicals, the dissociation limit of the lowest $^2\pi\sigma^*$ state is about 2.0 eV above the ground-state minimum. The PE functions of the bound ${}^2\pi\pi^*$ and ${}^2n\pi^*$ excited state as well as the PE function of the electronic ground state are predissociated by the repulsive PE function of the $^2\pi\sigma^*$ state, which opens a channel for fast (nonstatistical) H atom photodetachment. The photodetachment reaction restores the original chromophore (Py, Tz, or Hz), and part of the energy of the absorbed photon is preserved as chemical energy in the free H atom radical (see Scheme 1b).

Here, we discuss the spectrum of excited states and the excited-state PE functions for H atom detachment of the TClHzH, TCNHzH, and TAHzH radicals in comparison with the HzH radical. The vertical excitation energies and oscillator strengths (in parentheses) of the lowest seven excited states of the HzH, TClHzH, and TCNHzH radicals are listed in Table 4. For the significantly larger TAHzH radical, it was not

Table 4. Vertical Excitation Energies (in eV) of the Lowest Seven Excited States of the HzH, TClHzH, and TCNHzH Radicals Calculated with the Unrestricted ADC(2) Method^a

HzH	TClHzH	TCNHzH
$D_1 (\pi \pi^*) 1.59 (0.0031)$	$D_1 (\pi \pi^*) 1.39 (0.0034)$	$D_1 (\pi \pi^*) 1.40 (0.0088)$
$D_2 (\pi \pi^*) 1.83 (0.0088)$	$D_2 (\pi \pi^*) 1.64 (0.0106)$	$D_2 (\pi \pi^*) 1.73 (0.0130)$
$D_3 (\pi \sigma^*) 3.21 (0.0004)$	$D_3 (\pi \sigma^*) 3.33 (0.0013)$	$D_3 (\pi \pi^*) 2.94 (0.0202)$
$D_4 (\pi \pi^*) 3.40 (0.0112)$	$D_4 (\pi \pi^*) 3.59 (0.0140)$	$D_5 (\pi \pi^*) 3.29 (0.0413)$
$D_5 (\pi \pi^*) 3.64 (0.0377)$	$D_5 (\pi \pi^*) 3.73 (0.0426)$	D ₅ (nπ*) 3.42 (0.0000)
$D_6 (n\pi^*) 3.87 (0.0001)$	$D_6 (\pi \sigma^*) 3.86 (0.0000)$	$D_6 (n\pi^*) 3.66 (0.0004)$
$D_7 (\pi \pi^*) 3.89 (0.0028)$	$D_7 (n\pi^*) 3.95 (0.0000)$	$D_7 (\pi \pi^*) 3.66 (0.0010)$
		$D_n (\pi \sigma^*) 3.99 (0.0002)$

^aOscillator strengths are given in parentheses.

possible to obtain more than the three lowest excitation energies and oscillator strengths with the computational resources available to us. As expected for radicals, HzH and its derivatives possess low-lying excited states. The $^2\pi\pi^*$ states have low oscillator strengths, whereas the $^2n\pi^*$ and $^2\pi\sigma^*$ excited states are dark. The lowest $^2\pi\sigma^*$ excited state is the third excited state in the HzH, TClHzH, and TAHzH radicals. In the TCNHzH radical, the $^2\pi\sigma^*$ excited state is significantly higher in energy and is the eighth excited state at the ground-

state equilibrium geometry. In condensed aqueous environments, the $^2\pi\sigma^*$ states may be blue-shifted by several tenths of an electronvolt due to their Rydberg character at the ground-state equilibrium geometry.

The singly occupied molecular orbital (SOMO) is a π orbital for all radicals under consideration. The SOMO and the σ^* orbital of HzH are displayed in Figure 7. While the SOMO

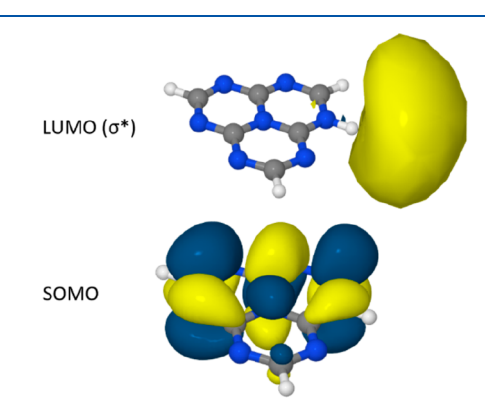


Figure 7. Singly occupied molecular orbital (SOMO) and the unoccupied diffuse σ^* orbital involved in the excitation of the $^2\pi\sigma^*$ state of the HzH radical. The diffuse σ^* orbital is mostly located outside the nuclear frame of the radical.

of HzH exhibits similarities with the LUMO of Hz (see Figure 2), the σ^* orbital is a diffuse orbital associated with the NH group of HzH. It exhibits a node (not visible in Figure 7 due to the diffuseness of the orbital) across the N–H bond. Most of its density is located outside the heteroaromatic ring. The population of the σ^* orbital in the $^2\pi\sigma^*$ excited state provides the driving force for the direct and fast detachment of the H atom. The shape of the σ^* orbital is similar for the three derivatives of HzH.

The PE profiles of the lowest electronic states of the HzH, TClHzH, TCNHzH, and TAHzH radicals as functions of the N-H bond length are displayed in Figure 8a-d. For clarity, the densely spaced PE functions of higher-lying $^2n\pi^*$ and $^2\pi\pi^*$ excited states are not included in the figure. For HzH, TClHzH, and TCNHzH, the lowest $^{2}n\pi^{*}$ PE function and the $^{2}\pi\pi^{*}$ PE functions below the lowest $^{2}n\pi^{*}$ PE function are included. For TAHzH, only the PE function of the $\pi\sigma^*$ state and the two lowest $\pi\pi^*$ excited states could be computed. While the PE functions of all $^2\pi\pi^*$ (green) and $^2n\pi^*$ (red) excited states are parallel to the PE function of the electronic ground state, the PE function of the $^2\pi\sigma^*$ excited state (blue) is dissociative with respect to the N–H bond. The $^2\pi\sigma^*$ state is essentially dark in all four radicals but can be populated by optical excitation to the densely spaced manifold of higherlying $^2\pi\pi^*$ states. In HzH, TClHzH, and TAHzH, the repulsive PE function of the $^2\pi\sigma^*$ state crosses the PE functions of two lower-lying $^2\pi\pi^*$ states as well as the PE function of the D₀ state (Figure 8a,b,d). In TCNHzH, however, the $^2\pi\sigma^*$ state is located higher in energy and its repulsive PE function crosses the bound PE functions of seven vertically lower-lying $\pi\pi^*$ and $n\pi^*$ excited states as well as the PE function of the D_0 state (Figure 8c). All these curve crossings become conical intersections when the out-of-plane vibrational modes are taken into account. Energy crossings of the $^2\pi\sigma^*$ state (A' symmetry) with the $^2\pi\pi^*$ states and with the D₀ state (A" symmetry) are symmetry allowed conical intersections, 31 while energy crossings of the $^2\pi\sigma^*$ state with $^2n\pi^*$ states are same-

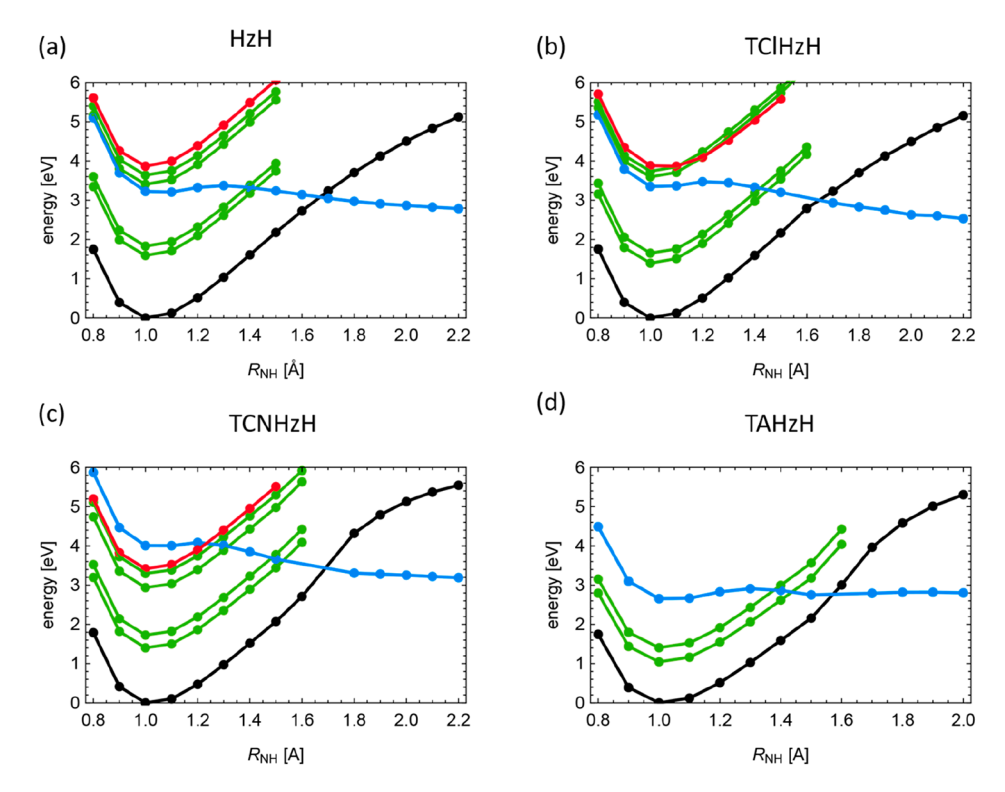


Figure 8. PE functions along the NH distance (R_{NH}) of the HzH (a), TClHzH (b), TCNHzH (c), and TAHzH (d) radicals. The PE function of the ground state is depicted in black. The PE functions of the $\pi\pi^*$ excited states are depicted in green and those of the $n\pi^*$ states in red. The repulsive $\pi\sigma^*$ state (blue) provides a reaction channel for photoinduced H atom detachment reaction. For clarity, only the lowest $n\pi^*$ state and the $\pi\pi^*$ states below this $n\pi^*$ state are included in (a)–(c). For TAHzH (d), only the PE functions of the reactive $\pi\sigma^*$ excited state and the two lowest $\pi\pi^*$ excited states could be computed with the available resources.

symmetry conical intersections. Since more conical intersections have to be passed diabatically in the photodissociation of the TCNHzH radical, it is expected that photodissociation yield of the TCNHzH radical is lower than that of the other radicals. *Ab initio* nonadiabatic quantum wave packet or quasiclassical surface-hopping simulations are necessary to obtain estimates of the photodissociation probability. A recent quantum wave packet computational study of the photodissociation of the PyH radical provided evidence that the photodissociation yield can be substantial.³⁶

The dissociation energy of the HzH radical has been computed as 2.0 eV at the CCSD level. This low dissociation energy implies that the dark recombination of two HzH radicals, yielding H₂ and regenerating two Hz molecules, is exothermic. This alternative photocatalytic scenario, which requires only two photons to generate one H₂ molecule, has been discussed in more detail by Ehrmaier et al. While more accurate calculations of the thermochemistry are necessary, the present results indicate that this reaction channel may be closed for the TCNHzH and TAHzH radicals, which exhibit higher dissociation energies than Hz (see Figure 8).

4. DISCUSSION AND CONCLUSIONS

In recent work, we explored the specific photochemistry of the Hz chromophore in the hydrogen-bonded Hz···H₂O complex²⁸ as well as in a computationally simulated aqueous solution, ¹⁷ by using wave function-based electronic-structure methods and DFT methods, respectively. The computational results reveal that the Hz molecule, when excited to the bright ${}^1\pi\pi^*$ state (S_5/S_6) , can abstract a hydrogen atom from the

hydrogen-bonded water molecule by electronic hole transfer (from Hz to H_2O), followed by the transfer of a proton from H_2O to Hz, resulting in the formation of the HzH···OH radical pair. Since the excess energy of this PCET reaction is substantial, the weak hydrogen bond of the HzH···OH radical pair is readily broken, yielding free HzH and OH radicals. In accordance with Kasha's rule, it is expected that the reaction mechanism involves ultrafast (a few femtoseconds) initial radiationless decay from the S_5/S_6 states via the intermediate $^1n\pi^*$ states (S_2, S_3, S_4) to the long-lived S_1 electronic state of Hz, which serves as a reservoir of excited Hz molecules. In this scenario, H atom abstraction occurs mainly by a barrier-controlled PCET reaction on the adiabatic S_1 PE surface.

In the present work, we explored the possibility of tuning the PCET reaction barrier by chemical substitution at the CH sites of the Hz chromophore, considering three selected derivatives of Hz. The results reveal that the excited-state reaction barrier can indeed be tuned by up to 0.5 eV, which is substantial, considering that the PCET rate depends exponentially on the barrier height. The results also reveal the electronic mechanism of this effect. While the vertical excitation energies of the LE $^{1}\pi\pi^{*}$ and $^{1}n\pi^{*}$ states of the Hz chromophore are weakly affected by the substituents (<0.5 eV, see Table 1), the vertical excitation energy of the (lowest) CT state varies by about 2.0 eV (from 6.15 eV for TAHz to 4.13 eV for TCNHz). The electron-donating anisole substituent raises the energy of the CT state, whereas the electron-withdrawing substituents Cl and CN lower the energy of the CT state. As is schematically shown in Figure 9, the vertical excitation energy of the CT state controls the height of the barrier on the adiabatic S₁ PE

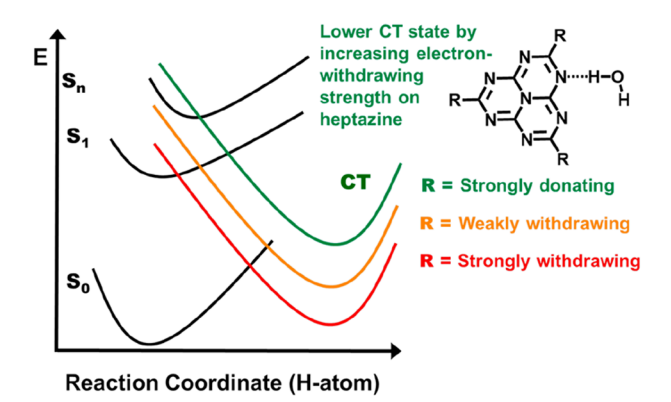


Figure 9. Pictorial energy landscape diagram for substituted $Hz \cdots H_2O$ complexes, illustrating the relationship between the vertical excitation energy of the CT state and the PCET barrier on the PE surface of the S_1 state.

surface, which results from a conical intersection of the CT state with the LE $S_1(\pi\pi^*)$ state. As a result of the vertical shift of the CT state, the PCET barrier in the $Hz\cdots H_2O$ complex (0.98 eV) is raised to 1.08 eV in the $TAHz\cdots H_2O$ complex, but is lowered to 0.80 eV for the weakly electron-withdrawing substituent Cl. For the strongly electron-withdrawing substituent CN, the barrier is lowered further to 0.59 eV; see Table 2. Electron-withdrawing substituents lead to a faster H atom abstraction reaction from the water molecule and therefore presumably to a higher quantum yield of the water oxidation reaction.

Quantitative experimental data on the PCET reaction are available for TAHz in aqueous solution. The exceptionally long fluorescence lifetime of TAHz in nonprotic solution (toluene) of 297 ns is reduced to 16 ns in aqueous solution. The rather high rate of PCET in TAHz···H2O may be due to the availability of vibrational excess energy from the initial internalconversion process in TAHz. Alternatively, the PCET reaction may also occur on the PE surfaces of the intermediately populated ${}^{1}n\pi^{*}$ states, which may exhibit lower barriers. To clarify these issues, dynamics simulations of the sequence of ultrafast nonadiabatic transitions within the chromophore and of the H atom transfer reaction are necessary. Recent nonadiabatic on-the-fly quasi-classical trajectory surface-hopping simulations with the TDDFT method for the complex of Hz with four water molecules provided tentative evidence of contributions of H atom transfer in higher electronic states (S_n, n > 1) to the overall reaction probability.¹⁸

The second crucial mechanistic element controlling the photoreactivity of Hz chromophores in aqueous environments is the seam of intersection of the adiabatic S₁ and S₀ PE surfaces, which is indicated by the black lines in Figure 4a-d. This seam of intersections acts as a bifurcation point for the photochemical dynamics. Part of the photoinduced quantum wave packet (or swarm of classical trajectories) will cross the conical intersection seam diabatically (staying on the PE surface of the CT state), while the other part will cross the seam adiabatically (staying on the adiabatic S_1 PE surface). The former part will yield the radical pair in a direct and fast reaction (successful H atom transfer), whereas the latter part most likely will convert to the electronic ground state of the complex after dissipation of the kinetic energy (aborted H atom transfer reaction). The dynamics at the conical seam is more complex than barrier-crossing or tunneling dynamics and

cannot be predicted just by the inspection of the topography of the PE surfaces. Nonadiabatic dynamics simulations of the type recently performed for $Py-(H_2O)_n$ clusters¹⁶ or $Hz-(H_2O)_n$ clusters¹⁸ are needed for the characterization of the reaction dynamics at the S_1-S_0 conical seam.

The photocatalytic cycle can be closed by photodetachment of the excess H atom from the reduced chromophore (see Scheme 1b). All reduced chromophores considered herein (HzH, TClHzH, TCNHzH, and TAHzH) possess a low-lying $^{2}\pi\sigma^{*}$ state, which is repulsive with respect to the N-H stretching coordinate. For all four radicals, the dissociation limit of the $^2\pi\sigma^*$ state is in the range 2.0–3.0 eV, much lower than the dissociation energy of the diabatic ground state (>5.0 eV). The conical intersection of the PE surface of the repulsive $^2\pi\sigma^*$ state with the bound PE surface of the D_0 state "cuts a hole" in the D₀ surface, which allows photodetachment of the excess H atom by a low-energy photon. The low-lying $^2\pi\pi^*$ states have rather small oscillator strengths but may borrow intensity from higher-lying strongly allowed $^2\pi\pi^*$ states. The detailed mechanisms of the photodetachment reaction and the dependence of the photodissociation rate on the photon energy require further exploration.

Our team recently showed that the ordering of the S₁ and T₁ excited states of Hz is inverted; that is, the S₁ state is lower in energy than the T₁ state by about 0.25 eV.³⁰ It was independently shown that cycl[3.3.3]azine, which is isoelectronic with heptazine, exhibits the same inversion of the S₁ and T_1 states.³⁷ The S_1/T_1 inversion is a unique property of Hz and systems isoelectronic with Hz. The peculiar nuclear geometry of Hz gives rise to HOMO and LUMO orbitals that are spatially nonoverlapping, which results in a near-zero exchange integral. Stabilization of the singlet state by spin-polarization then leads to an inverted singlet-triplet gap. 30 It was shown that the S_1/T_1 inversion of Hz is highly robust, being unaffected by chemical substitution as well as oligomerization. All four chromophores considered in the present work exhibit a negative singlet-triplet gap of about -0.25 eV. The S_1/T_1 inversion of Hz chromophores has two important consequences for photocatalysis. First, it eliminates intersystem crossing (ISC) as a channel for the quenching of the population of the S₁ state. Together with an exceptionally small transition dipole moment with the S₀ state, the lack of ISC gives rise to an exceptionally long lifetime of the S₁ state (297 ns for TAHz in toluene). The energy of the absorbed photon can thus be stored in the S₁ state of Hz chromophores on a time scale comparable to the time scale of molecular diffusion in liquids. Second, the absence of a long-lived triplet state in Hz chromophores eliminates the activation of triplet molecular oxygen to highly reactive and therefore detrimental singlet molecular oxygen. In contrast to transition-metal complexes, which generically possess long-lived triplet states that readily activate molecular oxygen, both the molecular photocatalyst TAHz³⁰ as well as the polymeric photocatalyst melon³⁸ were found to exhibit ultralow yields of singlet oxygen.

Water oxidation photocatalysis with Hz-based materials generates free OH radicals that have been detected either directly by electron spin resonance (ESR)⁴¹ or indirectly with fluorescent markers.^{9,42} While one goal is the efficient recombination of OH radicals to closed-shell H₂O₂, it may be unavoidable that some of the highly reactive OH radicals react with a reduced chromophore radical by radical–radical recombination, forming so-called photohydrates (see Scheme 1c).³³ We explored in the present work the thermochemistry of

Article

the photohydrates of Hz, TClHz, TCNHz, and TAHz. The thermochemistry of these photohydrates exhibits a clear trend: electron-withdrawing substituents stabilize the photohydrate, whereas electron-donation substituents destabilize the photohydrate. Specifically, the photohydrates of Hz, TClHz, and TCNHz are lower in energy than the corresponding chromophore-water complexes and therefore are thermodynamically stable. The photohydrate of TAHz, however, is higher in energy than the TAHz···H₂O complex by 5.77 kcal/ mol and therefore is thermodynamically metastable. It can convert back to the TAHz···H2O complex via a slow thermal reaction. These computational predictions are in agreement with the observation that Hz and TClHz hydrolyze readily in the presence of water, whereas TAHz is chemically stable under the same conditions,9 presumably due to the spontaneous decomposition of the metastable photohydrate, which is a self-healing process. Self-healing clearly is a highly desirable feature of any photocatalyst and is essential for longterm photostability. While the energy of the absorbed photon is wasted when the photohydration reaction occurs, the expensive photocatalyst is at least not destroyed by the reaction with OH radicals.

We computed the absorption spectra of the photohydrates of the four Hz species considered herein. The photohydrates exhibit a characteristic strong absorption band in the near UV. By this absorption band, the formation and decay of the photohydrates can be spectroscopically monitored. For molecular chromophores in solution, it may be possible to confirm that the formation of the photohydrate of TAHz is reversible, whereas the photohydration of Hz, TClHz, and TCNHz is irreversible. For polymeric Hz (melon), however, the spectroscopic detection of the photohydrate may be difficult, since presumably only a very low percentage of the bulk material can be photohydrated under UV/vis irradiation.

Finally, we point out that the vertical excitation energy of the CT state is a convenient proxy for the relative height of the PCET barrier on the adiabatic S₁ PE surface of different Hz··· H₂O complexes, as schematically indicated in Figure 9. The computation of the vertical excitation energy of the CT state is much faster and easier than the determination of the PCET barrier. While the determination of the saddle point requires tedious excited-state geometry optimization in a region where the electronic wave function switches its character (from LE to CT), the vertical excitation energy of the CT state is obtained by a straightforward single-point calculation at the ground-state equilibrium geometry. The relative energies of the photohydrates of different Hz···H2O complexes likewise are comparatively easy to evaluate by two ground-state geometry optimizations and single-point energy evaluations. With such easy-to-compute material parameters, extensive screening studies aiming at the identification of Hz-based chromophores with optimal photocatalytic efficiency and photostability should be possible.

ASSOCIATED CONTENT

Supporting Information

The Supporting Information is available free of charge at https://pubs.acs.org/doi/10.1021/acs.jpca.0c00488.

Cartesian coordinates of the saddle points of the PCET reaction on the S₁ PE surface of four Hz···H₂O complexes (PDF)

AUTHOR INFORMATION

Corresponding Author

Wolfgang Domcke - Department of Chemistry, Technical University of Munich, Garching D-85747, Germany; orcid.org/0000-0001-6523-1246; Email: domcke@ ch.tum.de

Authors

Johannes Ehrmaier - Department of Chemistry, Technical University of Munich, Garching D-85747, Germany

Xiang Huang - Department of Chemistry, Technical University of Munich, Garching D-85747, Germany

Emily J. Rabe – Department of Chemistry, University of Washington, Seattle, Washington 98195, United States; orcid.org/0000-0002-9397-049X

Kathryn L. Corp – Department of Chemistry, University of Washington, Seattle, Washington 98195, United States; orcid.org/0000-0002-2015-386X

Cody W. Schlenker – Department of Chemistry, University of Washington, Seattle, Washington 98195, United States; orcid.org/0000-0003-3103-402X

Andrzej L. Sobolewski – Institute of Physics, Polish Academy of Sciences, Warsaw PL-02-668, Poland; orcid.org/0000-0001-5718-489X

Complete contact information is available at: https://pubs.acs.org/10.1021/acs.jpca.0c00488

The authors declare no competing financial interest.

ACKNOWLEDGMENTS

This work has been supported by the Munich Centre for Advanced Photonics (MAP). J.E. acknowledges support by the International Max Planck Research School of Advanced Photon Science (IMPRS-APS). A.L.S. acknowledges support by the Alexander von Humboldt Research Award. C.W.S. acknowledges support by the National Science Foundation under Grant No. CHE-1846480

REFERENCES

- (1) Wang, X.; Maeda, K.; Thomas, A.; Takanabe, K.; Xin, G.; Carlsson, J. M.; Domen, K.; Antonietti, M. A Metal-Free Polymeric Photocatalyst for Hydrogen Production from Water Under Visible Light. Nat. Mater. 2009, 8, 76-80.
- (2) Ong, W.-J.; Tan, L.-L.; Ng, Y. H.; Yong, S.-T.; Chai, S.-P. Graphitic Carbon Nitride (g-C₃N₄)-Based Photocatalysts for Artificial Photosynthesis and Environmental Remediation: Are we a Step Closer to Achieving Sustainability? Chem. Rev. 2016, 116, 7159-
- (3) Wen, J.; Xie, J.; Chen, X.; Li, X. A Review on g-C₃N₄-Based Photocatalysts. Appl. Surf. Sci. 2017, 391, 72-123.
- (4) Rahman, M. Z.; Davey, K.; Qiao, S.-Z. Carbon, Nitrogen and Phosphorus Containing Metal-Free Photocatalysts for Hydrogen Production: Progress and Challenges. J. Mater. Chem. A 2018, 6, 1305-1322.
- (5) Wang, Y.; Wang, X.; Antonietti, M. Polymeric Graphitic Carbon Nitride as a Heterogeneous Organocatalyst: from Photochemistry to Multipurpose Catalysis to Sustainable Chemistry. Angew. Chem., Int. Ed. 2012, 51, 68-89.
- (6) Schwarzer, A.; Saplinova, T.; Kroke, E. Tri-s-Triazines (s-Heptazines) - From a "Mystery Molecule" to Industrially Relevant Carbon Nitride Materials. Coord. Chem. Rev. 2013, 257, 2032-2062.
- (7) Pauling, L.; Sturdivant, J. J. The Structure of Cyameluric Acid, Hydromelonic Acid, and Related Substances. Proc. Natl. Acad. Sci. U. S. A. 1937, 23, 615-620.

- (8) Hosmane, R. S.; Rossman, M. A.; Leonard, N. J. Synthesis and Structure of Tri-s-Triazine. J. Am. Chem. Soc. 1982, 104, 5497–5499.
- (9) Rabe, E. J.; Corp, K. L.; Sobolewski, A. L.; Domcke, W.; Schlenker, C. W. Proton-Coupled Electron Transfer from Water to a Model Heptazine-Based Molecular Photocatalyst. *J. Phys. Chem. Lett.* **2018**, *9*, 6257–6261.
- (10) Rabe, E. J.; Corp, K. L.; Huang, X.; Ehrmaier, J.; Flores, R. G.; Estes, S. L.; Sobolewski, A. L.; Domcke, W.; Schlenker, C. W. Barrierless Heptazine-Driven Excited-State Proton-Coupled Electron Transfer: Implications for Controlling Photochemistry of Carbon Nitrides and Aza-Arenes. *J. Phys. Chem. C* **2019**, *123*, 29580–29588.
- (11) Lau, V. W.-h.; Moudrakovski, I.; Botari, T.; Weinberger, S.; Mesch, M. B.; Duppel, V.; Senker, J.; Blum, V.; Lotsch, B. V. Rational Design of Carbon Nitride Photocatalysts by Identification of Cyanamide Defects as Catalytically Relevant Sites. *Nat. Commun.* **2016**, *7*, 12165.
- (12) Lau, V. W. h.; Klose, D.; Kasap, H.; Podjaski, F.; Pignié, M.-C.; Reisner, E.; Jeschke, G.; Lotsch, B. V. Dark Photocatalysis: Storage of Solar Energy in Carbon Nitride for Time-Delayed Hydrogen Generation. *Angew. Chem., Int. Ed.* **2017**, *56*, 510–514.
- (13) Yang, W.; Godin, R.; Kasap, H.; Moss, B.; Dong, Y.; Hillman, S. A. J.; Steier, L.; Reisner, R.; Durrant, J. R. Electron Accumulation Induces Efficiency Bottleneck for Hydrogen Production in Carbon Nitride Photocatalysts. *J. Am. Chem. Soc.* **2019**, *141*, 11219–11229.
- (14) Wen, J.; Li, R.; Lu, R.; Yu, A. Photophysics and Photocatalysis of Melem: A Spectroscopic Reinvestigation. *Chem. Asian J.* **2018**, *13*, 1060–1066.
- (15) Pang, X.; Ehrmaier, J.; Wu, X.; Jiang, C.; Xie, W.; Sobolewski, A. L.; Domcke, W. Photoinduced Hydrogen-Transfer Reactions in Pyridine-Water Clusters: Insights From Excited-State Electronic-Structure Calculations. *Chem. Phys.* **2018**, *515*, 550–556.
- (16) Pang, X.; Jiang, C.; Xie, W.; Domcke, W. Photoinduced Electron-Driven Proton Transfer from Water to an N-Heterocyclic Chromophore: Nonadiabatic Dynamics Studies for Pyridine-Water Clusters. *Phys. Chem. Chem. Phys.* **2019**, 21, 14073–14079.
- (17) Ehrmaier, J.; Domcke, W.; Opalka, D. Mechanism of Photocatalytic Water Oxidation by Graphitic Carbon Nitride. *J. Phys. Chem. Lett.* **2018**, *9*, 4695–4699.
- (18) Ullah, N.; Chen, S.; Zhao, Y.; Zhang, R. Photoinduced Water-Heptazine Electron-Driven Proton Transfer: Perspective for Water Splitting With g-C₃N₄. J. Phys. Chem. Lett. **2019**, 10, 4310–4316.
- (19) Møller, C.; Plesset, M. S. Note on an Approximation Treatment for Many-Electron Systems. *Phys. Rev.* **1934**, *46*, 618–622.
- (20) Schirmer, J. Beyond the Kandom-Phase Approximation: A New Approximation Scheme for the Polarization Propagator. *Phys. Rev. A: At., Mol., Opt. Phys.* **1982**, *26*, 2395–2416.
- (21) Liu, X.; Sobolewski, A. L.; Borrelli, R.; Domcke, W. Computational Investigation of the Photoinduced Homolytic Dissociation of Water in the Pyridine–Water Complex. *Phys. Chem. Chem. Phys.* **2013**, *15*, 5957–5966.
- (22) Ehrmaier, J.; Janicki, M. J.; Sobolewski, A. L.; Domcke, W. Mechanism of Photocatalytic Water Splitting With Triazine-Based Carbon Nitrides: Insights From Ab Initio Calculations on the Triazine-Water Complex. *Phys. Chem. Chem. Phys.* **2018**, 20, 14420—14430.
- (23) Liu, X.; Sobolewski, A. L.; Domcke, W. Photoinduced Oxidation of Water in the Pyridine–Water Complex: Comparison of the Singlet and Triplet Photochemistries. *J. Phys. Chem. A* **2014**, *118* (36), 7788–7795.
- (24) Starcke, J. H.; Wormit, M.; Dreuw, A. Unrestricted Algebraic Diagrammatic Construction Scheme of Second Order for the Calculation of Excited States of Medium-Sized and Large Molecules. *J. Chem. Phys.* **2009**, *130*, 024104.
- (25) Dunning, T. H., Jr. Gaussian Basis Sets for Use in Correlated Molecular Calculations. I. The Atoms Boron Through Neon and Hydrogen. J. Chem. Phys. 1989, 90, 1007–1023.
- (26) TURBOMOLE (V. 6.3); a development of University Karlsruhe and Forschungszentrum Karlsruhe GmbH, 1989–2007.

- (27) Hättig, C.; Weigend, F. CC2 Excitation Energy Calculations on Large Molecules Using the Resolution of the Identity Approximation. *J. Chem. Phys.* **2000**, *113*, 5154–5161.
- (28) Ehrmaier, J.; Karsili, T. N. V.; Sobolewski, A. L.; Domcke, W. Mechanism of Photocatalytic Water Splitting with Graphitic Carbon Nitride: Photochemistry of the Heptazine–Water Complex. *J. Phys. Chem. A* **2017**, *121*, 4754–4764.
- (29) Kollmar, H.; Staemmler, V. Violation of Hund's Rule by Spin Polarization in Molecules. *Theoret. Chim. Acta (Berl.)* **1978**, 48, 223–239
- (30) Ehrmaier, J.; Rabe, E. J.; Pristash, S. R.; Corp, K. L.; Schlenker, C. W.; Sobolewski, A. L.; Domcke, W. Singlet-Triplet Inversion in Heptazine and in Polymeric Carbon Nitrides. *J. Phys. Chem. A* **2019**, 123, 8099–8108.
- (31) Domcke, W.; Yarkony, D. R.; Köppel, H. Conical Intersections: Electronic Structure, Dynamics and Spectroscopy; World Scientific: Singapore, 2004.
- (32) Domcke, W.; Ehrmaier, J.; Sobolewski, A. L. Solar Energy Harvesting with Carbon Nitrides and N-Heterocyclic Frameworks: Do We Understand the Mechanism? *ChemPhotoChem.* **2019**, *3*, 10–23
- (33) Wilzbach, K. E.; Rausch, D. J. Photochemistry of Nitrogen Heterocycles. Dewar Pyridine and Its Intermediacy in Photoreduction and Photohydration of Pyridine. *J. Am. Chem. Soc.* **1970**, 92, 2178–2179.
- (34) Joussot-Dubien, J.; Houdard, J. Reversible Photolysis of Pyridine in Aqueous Solution. *Tetrahedron Lett.* **1967**, *8*, 4389–4391.
- (35) Andre, J. C.; Niclause, M.; Joussot-Dubien, J.; Deglise, X. Photohydration of Pyridine in Aqueous Solution. *J. Chem. Educ.* **1977**, *54*, 387–388.
- (36) Ehrmaier, J.; Picconi, D.; Karsili, T. N. V.; Domcke, W. Photodissociation Dynamics of the Pyridinyl Radical: Time-Dependent Quantum Wave-Packet Calculations. *J. Chem. Phys.* **2017**, *146*, 124304.
- (37) de Silva, P. Inverted Singlet-Triplet Gaps and Their Relevance to Thermally Activated Delayed Fluorescence. *J. Phys. Chem. Lett.* **2019**, *10*, 5674–5679.
- (38) Cui, Y.; Ding, Z.; Liu, P.; Antonietti, M.; Fu, X.; Wang, X. Metal-Free Activation of H_2O_2 by $g-C_3N_4$ under Visible Light Irradiation for the Degradation of Organic Pollutants. *Phys. Chem. Phys.* **2012**, *14*, 1455–1462.
- (39) Chen, Y.; Zhang, J.; Zhang, M.; Wang, X. Molecular and Textural Engineering of Conjugated Carbon Nitride Catalysts for Selective Oxidation of Alcohols with Visible Light. *Chem. Sci.* **2013**, *4*, 3244–3248.
- (40) Wang, H.; Jiang, S.; Chen, S.; Li, D.; Zhang, X.; Shao, W.; Sun, X.; Xie, J.; Zhao, Z.; Zhang, Q. Enhanced Singlet Oxygen Generation in Oxidized Graphitic Carbon Nitride for Organic Synthesis. *Adv. Mater.* **2016**, *28*, 6940–6945.
- (41) Yang, Y.; Chen, J.; Mao, Z.; An, N.; Wang, D.; Fahlmann, B. D. Ultrathin g-C₃N₄ Nanosheets With an Extended Visible-Light-Responsive Range for Significant Enhancement of Photocatalysis. *RSC Adv.* **2017**, *7*, 2333–2341.
- (42) Nagarajan, S.; Skillen, N. C.; Fina, F.; Zhang, G.; Random, C.; Lawton, N. A.; Irvine, J. T. S.; Robertson, P. K. J. Comparative Assessment of Visible Light and UV Active Photocatalysts by Hydroxyl Radical Quantification. *J. Photochem. Photobiol., A* **2017**, 334, 13–19.